2014

Form Factor of pNIPAM Microgels in Overpacked States

U. Gasser
Paul Scherrer Institute

J. S. Hyatt
Georgia Institute of Technology

J.- J. Lietor-Santos
Georgia Institute of Technology

E. S. Herman
Georgia Institute of Technology

L. Andrew Lyon
Chapman University, lyon@chapman.edu

See next page for additional authors

Recommended Citation
Gasser U.; Hyatt J. S.; Lietor-Santos, J. J.; Herman E. S.; Lyon, L. A.; Fernandez-Nieves A., Form factor of pNIPAM microgels in overpacked states, *J. Chem. Phys.*, 2014, 141(3), 034901.
DOI: 10.1063/1.4885444

Form Factor of pNIPAM Microgels in Overpacked States

Authors
U. Gasser, J. S. Hyatt, J.- J. Lietor-Santos, E. S. Herman, L. Andrew Lyon, and A. Fernandez-Nieves

Form factor of pNIPAM microgels in overpacked states

U. Gasser,[1,a)] J. S. Hyatt,[2] J.-J. Lietor-Santos,[2] E. S. Herman,[3] L. A. Lyon,[3] and A. Fernandez-Nieves[2,b)]

[1]*Laboratory for Neutron Scattering and Imaging, Paul Scherrer Institut, 5232 Villigen, Switzerland*
[2]*School of Physics, Georgia Institute of Technology, Atlanta, Georgia 30332-0430, USA*
[3]*School of Chemistry and Biochemistry, Georgia Institute of Technology, Atlanta, Georgia 30332-0400, USA*

(Received 10 December 2013; accepted 16 June 2014; published online 18 July 2014)

We study the form factor of thermoresponsive microgels based on poly(*N*-isopropylacrylamide) at high generalized volume fractions, ζ, where the particles must shrink or interpenetrate to fit into the available space. Small-angle neutron scattering with contrast matching techniques is used to determine the particle form factor. We find that the particle size is constant up to a volume fraction roughly between random close packing and space filling. Beyond this point, the particle size decreases with increasing particle concentration; this decrease is found to occur with little interpenetration. Noteworthily, the suspensions remain liquid-like for ζ larger than 1, emphasizing the importance of particle softness in determining suspension behavior. © *2014 AIP Publishing LLC*. [http://dx.doi.org/10.1063/1.4885444]

INTRODUCTION

Microgel particles are cross-linked polymer networks with diameters in the nm- to μm-range. They can change size in response to variations in temperature,[1] hydrostatic pressure,[2] *p*H,[3] salt concentration,[4] and external osmotic pressure.[5] This transition between swollen and deswollen states is attractive for many applications.[6–9] In addition, since changes in the microgel size also induce changes in the suspension volume fraction, this swelling transition has also been exploited in fundamental studies related to phase transitions[10] and glass formation.[11]

The macroscopic behavior of the suspension is largely determined by the particle concentration and by interparticle interactions. However, the properties of the particles can also play an important role. In fact, the elastic scale of emulsions and foams is set by the value of interfacial tension and the droplet or bubble size, which is the characteristic length scale in these systems; it is the energy stored at the interfaces, when the droplets are deformed at high packing fractions, that determines the elastic response of these materials.[12–14] For disordered suspensions of hard spheres, whose interactions and phase behavior are solely dictated by excluded volume, the elasticity results from changes in the equilibrium configuration of the particles when caged by their neighbors in the glassy phase.[15]

Colloidal microgels are different from drops, bubbles, and hard spheres for two main reasons: (i) they are compressible[16,17] and (ii) can potentially interpenetrate to some extent due to the presence of dangling polymer chains at their periphery.[18] They are, however, also potentially able to change shape like drops and bubbles.[16,19] A direct consequence of these particularities is that the energetic penalty for close interparticle approaches is not prohibitively large, hence allowing particle concentrations far beyond those that can be typically reached with emulsions, foams, and hard sphere suspensions. Perhaps not surprisingly, then, the relative viscosity of many microgel suspensions exhibits a much more gradual increase at high volume fractions than hard sphere suspensions.[11,20–22] For ionic microgels, this has been explained in terms of ion-induced deswelling. With increasing particle concentration the available volume for ions outside the particles decreases while the associated osmotic pressure increases; this can result in particle deswelling at volume fractions well below random close packing.[23–26] Recent experiments, however, find no significant ion-induced deswelling and a microgel size that only decreases at volume fractions above random close packing;[17,27] the inhomogeneous monomer distribution inside these microgels helps account for this difference in behavior.[27]

For neutral microgels, deswelling at low volume fractions was considered to understand the structural properties of dense suspensions.[28] However, recent experiments with glass-forming microgel suspensions did not consider deswelling at low volume fractions to interpret the measured fragility of a microgel glass in terms of the single-particle stiffness.[11]

In this paper we examine the rheology and structure of neutral poly(*N*-isopropylacrylamide) (pNIPAM) microgel suspensions with generalized volume fractions ranging from dilute to overpacked conditions. We use small-angle neutron scattering (SANS) to study the internal structure and the single-particle size of these microgels and find no deswelling up to generalized volume fractions, ζ, of approximately 1, followed by shrinking with slight particle interpenetration at higher ζ; this indicates that the particles are deswelling only after they are in contact with each other. Rheology of the suspensions confirms the relevance of particle softness: the suspensions remain liquid-like for ζ above 1, supporting the idea that it is the single-particle softness that is responsible for the behavior of concentrated suspensions of neutral microgels.

a)urs.gasser@psi.ch
b)alberto.fernandez@physics.gatech.edu

EXPERIMENTAL METHODS

pNIPAM microgel particles

We use hydrogenated and deuterated microgel particles to determine the particle form factor by SANS, taking advantage of contrast variation with H_2O/D_2O mixtures as solvent. We synthesize the hydrogenated particles using the NIPAM monomer $C_6H_{11}NO$ (H-NIPAM), which has a molecular weight of 113.16 g/mol, and the deuterated particles using the monomer $C_6H_4D_7NO$ (D-NIPAM), which has a molecular weight of 120.21 g/mol. Here, D represents deuterium, ^{2}H. The deuteration level of the D-NIPAM is 64%.

We follow a dispersion polymerization synthesis according to previously published methods.[29] All reagents are bought from Sigma Aldrich, except for the D-NIPAM monomer, which is bought from Polymer Source. For the synthesis of the H-NIPAM particles, we add 2.218 g of NIPAM, 0.062 g (2.0 mol. %) of the crosslinker *N,N′*-methylenebisacrylamide (BIS, $C_7H_{10}N_2O_2$), 0.072 g of surfactant sodium dodecyl sulfate (SDS), and 0.059 g of initiator ammonium persulfate [$(NH_4)_2S_2O_8$] to 250 ml distilled and deionized water at $(70 \pm 2)\,^\circ$C. We allow the reaction to proceed for 14 h while stirring at 450 rpm. The dispersion is then cooled to room temperature and aggregates are removed by filtering the product through Watman paper (pore size 42.5 μm). To remove unreacted monomer, cross-linker, surfactant, and initiator molecules, we centrifuge the suspension at 70 000 rpm (266×10^3 g) for 20 min at $(20 \pm 2)\,^\circ$C. After removing the supernatant, we resuspend the particles in distilled and deionized water, and repeat the process twice. For synthesis of the D-NIPAM particles, the procedure is the same, except that the amounts are 1.414 g of D-NIPAM, 0.037 g (2.0 mol. %) of BIS, 0.058 g of SDS, 0.058 g of ammonium persulfate, and 100 ml of distilled and deionized water; additionally, we allow the reaction to proceed for 22 h while stirring at 400 rpm and perform each centrifugation cycle for 1 h at 100 000 rpm (542×10^3 g).

We determine the swelling behavior of the particles using dynamic light scattering (DLS), in which we measure the time-dependent intensity fluctuations of light scattered from the sample. The timescale of these fluctuations allows us to determine the diffusion coefficient, D, of the particles; we then calculate their hydrodynamic radius, R_H, from the Stokes-Einstein equation, $D = k_BT/(6\pi\eta_s R_H)$, with k_B the Boltzmann constant, T the temperature, and η_s the solvent viscosity.[30,31] We observe that the particles start to appreciably deswell at $T \approx 32\,^\circ$C, for the H-NIPAM particles in H_2O, and at $T \approx 35\,^\circ$C, for the D-NIPAM particles in D_2O [see Fig. 1]. The higher deswelling temperature for the suspension in D_2O than for the suspension in H_2O agrees with previous observations.[32–34]

Due to the softness of swollen microgel particles, the relationship between polymer concentration, c_p, and particle volume fraction is not as straightforward as for hard particles. Indeed, suspensions of microgels can be concentrated beyond the highest possible volume fraction of hard particles since microgels can deform and deswell as their concentration is increased. As a result, instead of the volume fraction ϕ, we use a generalized volume fraction, $\zeta = nV_{p,d}$, where n is the particle number density and $V_{p,d}$ is the volume of one particle in a dilute suspension.

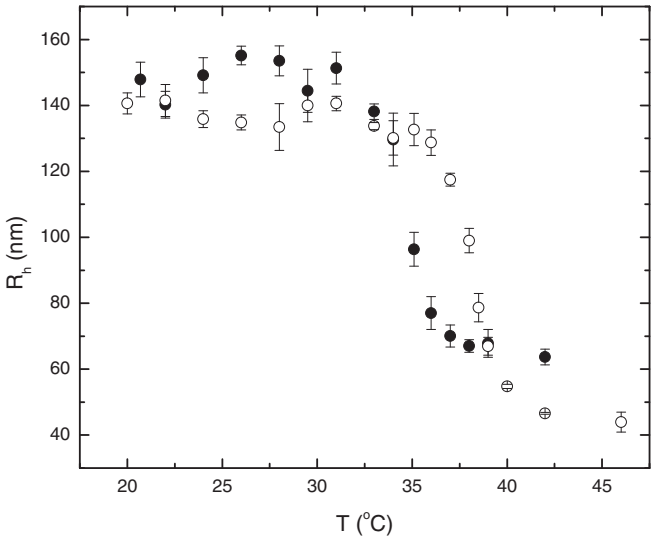

FIG. 1. Hydrodynamic radius, R_H, determined by DLS versus temperature for H-NIPAM particles in H_2O (filled circles) and D-NIPAM particles in D_2O (open circles).

We define $\zeta_H = k_H c_{p,H}$ as the generalized volume fraction of H-NIPAM microgels, where $c_{p,H}$ is the weight fraction of the H-NIPAM microgel suspension and k_H is a constant of proportionality. To determine k_H we measure the viscosity of dilute suspensions of H-NIPAM microgels in H_2O at different concentrations and fit the data to the Einstein-Batchelor equation, $\eta = \eta_{solvent}\,(1 + 2.5\zeta + 5.9\zeta^2)$, leaving k_H as fitting parameter. This procedure is, in principle, valid only for dilute hard sphere suspensions. However, since microgels are hydrodynamically opaque,[35] it is also applicable to suspensions of microgel particles. From the fit, shown in Fig. 2(a), we obtain $k_H = 22.4 \pm 0.6$. The generalized volume fraction of D-NIPAM microgels, $\zeta_D = k_D c_{p,D}$, is similarly obtained from the viscometry of dilute suspensions of D-NIPAM microgels in D_2O, as shown in Fig. 2(b). We obtain $k_D = 51 \pm 1$. All viscometry is carried out at $T = (20.0 \pm 0.1)\,^\circ$C. For suspensions containing both H- and D-NIPAM particles, we define the total generalized volume fraction as $\zeta = k_H c_{p,H} + k_D c_{p,D}$.

In order to prepare the concentrated samples, we resuspend freeze-dried microgels in mixtures of H_2O and D_2O at the desired weight fraction. In order to facilitate mixing, we heat the suspensions to deswell the microgels; this reduces the volume fraction, appreciably decreasing the suspension viscosity. Once mixed, we cool back to room temperature. This allows us to obtain homogeneous suspensions with $\zeta > 1$.

Rheology

We perform steady-state and oscillatory rheology with a stress-controlled rheometer (Anton-Paar, Physica MCR 501), using cone-plate geometry. The cone has a 25 mm diameter and a 2° aperture and is roughened. The instrument is calibrated to account for different sources of error: (i) motor and air bearing noise due to imperfections in motor

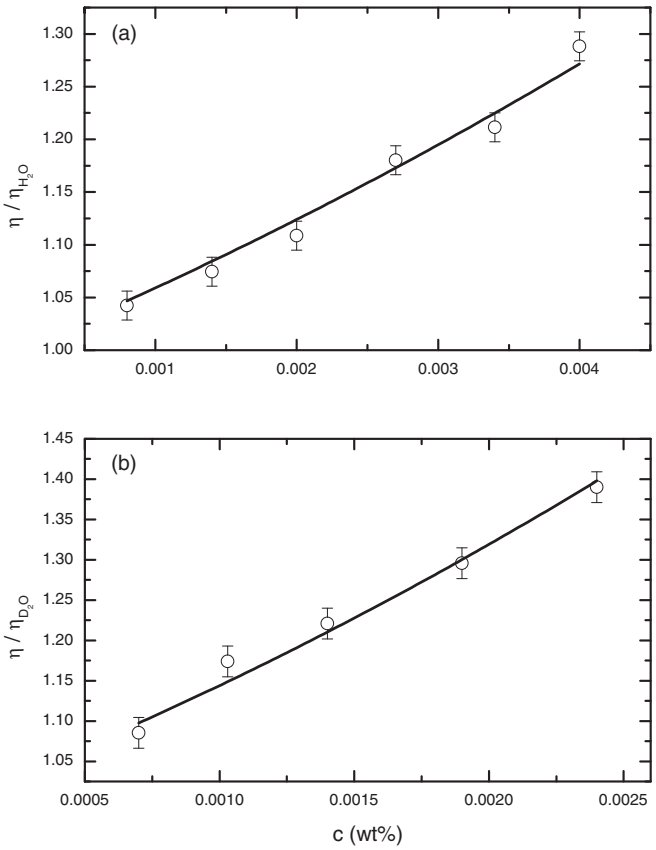

FIG. 2. Relative viscosity vs. microgel mass fraction for (a) H-NIPAM microgels in water and (b) D-NIPAM microgels in heavy water. Solid lines are fits to the Einstein-Batchelor equation. The coefficients obtained from the fits are $k_H = 22.4 \pm 0.6$ and $k_D = 51 \pm 1$. The measurements are performed at $T = (20.0 \pm 0.1)\,^{\circ}$C.

operation and turbulence in the air bearing, and (ii) the effect of inertia on stress. We make all measurements well above the minimum torque limit of the instrument, 0.1μNm. The oscillatory strain-controlled measurements are performed on timescales longer than the feedback loop time of the rheometer, ~1 ms. The temperature for all measurements is $(21 \pm 2)\,^{\circ}$C. We perform linearity tests at 10 rad/s for strains in the range [0.001,0.01] to ensure that oscillatory measurements are made in the linear regime. We also note that although glassy microgel systems display aging behavior,[36–39] we do not observe any history dependence in our measurements.

SANS

We use two methods to determine the particle form factor at high concentrations. (i) The "tracer" method is an analog to a form factor measurement under dilute conditions: A small amount of H-NIPAM particles is immersed in a "sea" of D-NIPAM particles that are contrast-matched with the H_2O / D_2O solvent. This allows for a direct measurement of the form factor of the H-NIPAM particles, $P_H(q)$, at arbitrarily large ζ. (ii) The zero average contrast (ZAC) method[40,41] allows us to determine the form factor with a sample corresponding to a 50/50 mol. % blend of H- and D-NIPAM in H_2O / D_2O solvent with a scattering length density given by the average scattering length density of the H- and D-NIPAM in the sample. Under these conditions, the coherent interparticle scattering cancels out and only the form factors $P_H(q)$ and $P_D(q)$ contribute to the coherent scattering through the average form factor $P_{ZAC}(q) = (P_H(q) + P_D(q))/2$.

An accurate knowledge of the coherent neutron scattering length densities of H- and D-NIPAM particles is needed to achieve the required contrast matching conditions for the tracer or the ZAC method. If microgels are suspended in a solvent that matches their scattering length density, they will not contribute to the coherent scattering of the sample. The scattering length densities (SLDs) of H_2O and D_2O are well-known quantities, $\mathrm{SLD}_{H_2O} = -0.56 \times 10^{-6}$ Å^{-2} and $\mathrm{SLD}_{D_2O} = 6.33 \times 10^{-6}$ Å^{-2}.[42] The SLD of an H_2O/D_2O mixture is given by $\mathrm{SLD}_{\mathrm{mixture}} = \mathrm{v}_{H_2O} \times \mathrm{SLD}_{H_2O} + \mathrm{v}_{D_2O} \times \mathrm{SLD}_{D_2O}$, where v_{H_2O} and v_{D_2O} are the volume fractions of H_2O and D_2O in the mixture.

In order to prepare samples with the right contrast matching, we first estimate the microgel SLD using established values for the scattering length of different elements[43] and the molecular formulas for H- and D-NIPAM and BIS, using 98 wt. % of NIPAM and 2 wt. % of BIS for each case, and from estimates of their densities. The density of H-NIPAM is $\rho_{H\text{-}NIPAM} = 1.100$ g/cm^3.[44] We then calculate the density of D-NIPAM by multiplying this value with the ratio of the molecular weights of D- and H-NIPAM to obtain $\rho_{D\text{-}NIPAM} = 1.167$ g/cm^3. With this information, we obtain $\mathrm{SLD}_{\mathrm{H-NIPAM}} = 0.838 \times 10^{-6}$ Å^{-2} and $\mathrm{SLD}_{\mathrm{D-NIPAM}} = 4.98 \times 10^{-6}$ Å^{-2}.

We also measure the microgel scattering length densities experimentally by suspending H- and D-NIPAM microgels in different mixtures of H_2O and D_2O and looking for the mixture resulting in no scattering; this corresponds to the so-called matchpoint of the system. The number of neutrons scattered into a solid angle element of the detector $\Delta\Omega$ in time Δt at a given scattering wave vector q is given by[45]

$$I_s(q) = \Phi_0 \Delta\Omega \Delta t \frac{T_s}{T_{empty}} a D_s \epsilon(\lambda) \frac{d\Sigma_V}{d\Omega}(q), \qquad (1)$$

where Φ_0 is the incident neutron flux or number of neutrons per unit area and unit time that are incident on the sample, T_s and T_{empty} are the transmissions of the sample and empty cell, respectively, a is the illuminated sample area, D_s is the sample thickness, $\epsilon(\lambda)$ is the efficiency of the detector at neutron wavelength λ, and $d\Sigma_V/d\Omega$ is the differential scattering cross section per unit volume. The latter is related to the differential scattering cross section per unit mass as $d\Sigma_m/d\Omega = (d\Sigma_V/d\Omega)/c_s$, where c_s is the sample concentration in mass per volume. The differential scattering cross section per particle can be further obtained as $d\Sigma_M/d\Omega = m_p(d\Sigma_m/d\Omega)$, with m_p the mass of one particle. At zero scattering wave vector,[45]

$$\frac{d\Sigma_M}{d\Omega}(q = 0) = (\Delta\rho_p \bar{v}_p m_p)^2, \qquad (2)$$

where $\Delta\rho_p$ is the difference in scattering length density between the particle and the solvent or the SLD contrast and $\bar{v}_p$ is the (dry) specific volume of the particles. Combining Eqs. (1) and (2) and factoring out a constant

$K = (T_{empty}/T_s)/(\Phi_0 a D_s \epsilon(\lambda)\Delta\Omega\Delta t)$ gives

$$\Delta\rho_p = \sqrt{\frac{K}{c_s m_p \bar{v}_p^2} I_s(q=0)}. \quad (3)$$

Approximating $\bar{v}_p \approx \rho_p^{-1}$, where ρ_p is the density of a single microgel particle, and assuming that the volume of a single particle does not change, which is true in the experiments for determining the particle SLD matchpoint, Eq. (3) is further simplified to

$$\Delta\rho_p \propto \sqrt{\frac{I_s(q=0)}{\phi}}, \quad (4)$$

where ϕ is the particle volume fraction.

To experimentally determine the matchpoint, we measure the scattered intensity as a function of q and plot it as a function of q^2 in a log-lin form. In this way, the data scale linearly, as shown in Figs. 3(a) and 3(b) for H- and D-NIPAM particles, and consistent with what is expected in the Guinier regime.[46] We then perform linear fits to the data to obtain the intercept, $I_s(q=0)$, for different H_2O-D_2O mixtures, normalize it with the particle volume fraction and plot the square root of the result against the SLD of the mixture [see Fig. 4]. We note that while $\Delta\rho_p$ changes sign for samples above the matchpoint, $I_s(q=0)$ increases with $\Delta\rho_p$ on both sides of the matchpoint [see Eq. (2)]. As a result, the H-microgel point with $SLD_{mixture} = -0.56 \times 10^{-6}$ Å^{-2} and the D-microgel point with $SLD_{mixture} = 6.33 \times 10^{-6}$ Å^{-2} both had their signs manually reversed in Fig. 4. After taking this into account, we find a linear relation between $\sqrt{I_s(q=0)/\phi}$ and $SLD_{mixture}$, as shown in Figs. 4(a) and 4(b) for H- and D-NIPAM microgels, respectively. The roots of the corresponding linear fits give the $SLD_{mixture}$ at the matchpoints, which are equal to the SLD of the particles. We find

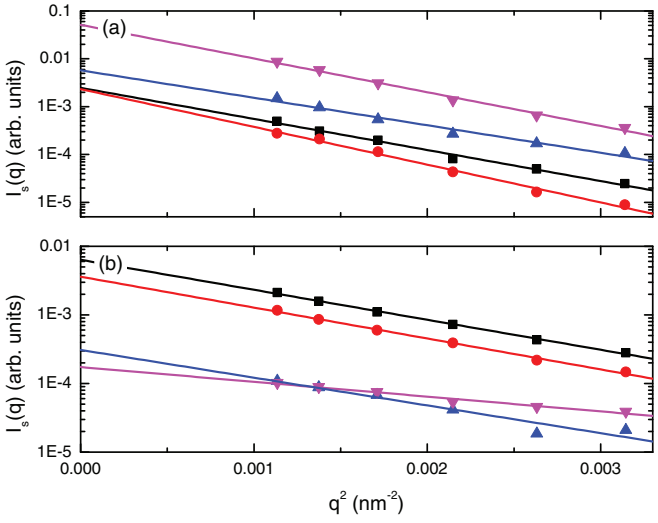

FIG. 3. Plots of the low-q region of $I_s(q)$ versus q^2 for (a) H-NIPAM microgels and (b) D-NIPAM microgels, extrapolated to $q = 0$. Proportions of solvent are given in wt. $\%_{H_2O}$/wt. $\%_{D_2O}$ as follows: (a) 100/0 (black squares), 54/46 (red circles), 32/68 (blue upward triangles), and 0/100 (magenta downward triangles); (b) 96.5/3.5 (black squares), 75.6/24.4 (red circles), 39.0/61.0 (blue upward triangles), and 0/100 (magenta downward triangles).

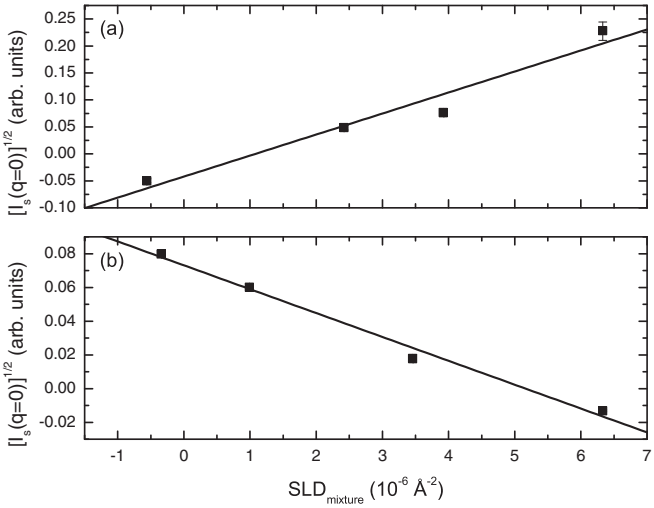

FIG. 4. Plots of $\sqrt{I_s(q=0)/\phi}$ versus the solvent SLD for (a) H-NIPAM microgels and (b) D-NIPAM microgels. The H-microgel point with $SLD_{mixture} = -0.56 \times 10^{-6}$ Å^{-2} and the D-microgel point with $SLD_{mixture} = 6.33 \times 10^{-6}$ Å^{-2} both had their signs reversed in order to account for the fact that the scattering contrast increases to either side of the matchpoint with the same magnitude of slope. The lines are linear fits used to determine the matchpoint, which corresponds to $I_s(q) = 0$.

$SLD_{H-NIPAM} = (1.1 \pm 0.8) \times 10^{-6}$ Å^{-2} and $SLD_{D-NIPAM} = (5.2 \pm 0.6) \times 10^{-6}$ Å^{-2}. These values agree with the calculated SLD of both H- and D-NIPAM particles.

Using the experimentally determined scattering length densities, we prepare the H_2O / D_2O mixtures for tracer and ZAC experiments by matching the scattering length density of the mixture to the D-NIPAM particles (tracer method) or to a 50/50 blend of H- and D-NIPAM particles (ZAC method).

For the form factor measurements of our particles on the SANS-I beam line at SINQ (Paul Scherrer Institut, Switzerland), we place the detector at a distance of 18 m from the sample and use a wavelength of 8 Å. To gain access to higher q-values, we also use a second setting with a sample-detector distance of 4.5 m. We collect the scattered intensity with a ^{3}He area detector with 128 × 128 pixels and a pixel size of 7.5 mm and use standard procedures to correct for dark counts, background scattering due to the quartz cuvettes, and the solvent.[47] The detector efficiency is calibrated using a H_2O measurement. For the analysis of the measured form factors, the q-resolution of the instrument is taken into account. We calculate the relative error in q, $\delta q/q = \delta\lambda/\lambda + \delta\theta/\theta$, from the relative wavelength spread, $\delta\lambda/\lambda = 0.1$, and the detector resolution at each scattering angle, $\delta\theta/\theta$, which depends on the sample-detector distance and the lateral distance from the direct beam position.

RESULTS AND DISCUSSION

SANS of dilute suspensions

We determine the form factor under dilute conditions for both H-NIPAM particles suspended in H_2O and D-NIPAM particles suspended in D_2O. The results are qualitatively similar to each other and similar to what has been previously reported for other pNIPAM-microgel suspensions,[48,49] with the

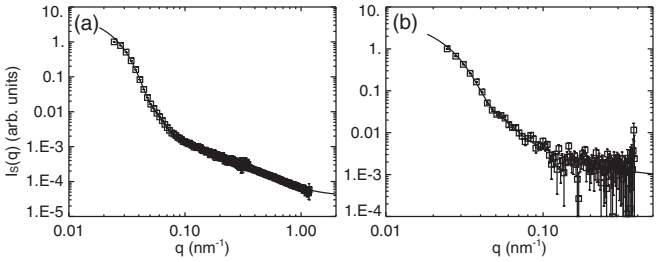

FIG. 5. Measured form factors of dilute samples (open squares) and corresponding fits (lines) to Eqs. (6) and (8). The samples are (a) H1 and (b) D1 from Table I. The first point in each measured form factor is slightly lower than its actual value due to incomplete masking of the beamstop. We accordingly perform our fits giving less statistical weight to this first point.

scattered intensity monotonously decreasing with q, as shown in Fig. 5. We analyze the results using the model introduced by Stieger *et al.*[28,48,50] This model treats a microgel particle as a spherical core with a certain fuzziness at its periphery essentially arising from the inhomogeneous distribution of cross-linker within the particle. This is modeled in real space as a convolution of a compact sphere with a Gaussian generating the fuzzy shell. The core radius, R_c, and the width of the Gaussian, σ, are treated as fitting parameters, and the effective particle radius is obtained as $R_{\mathrm{SANS}} = R_c + 2\sigma$. The form factor is given by

$$P_1(q) = \left[\frac{3(\sin q R_c - q R_c \cos q R_c)}{(q R_c)^3} \exp\left(-\frac{(\sigma q)^2}{2}\right)\right]^2. \tag{5}$$

Polydispersity in the core, σ_p, is taken into account with a Gaussian size distribution such that the average form factor is obtained as

$$P(q) = \frac{1}{\sqrt{2\pi}\sigma_p \langle R_c\rangle \langle V^2\rangle} \int dR_c V^2(R_c) P_1(q, R_c) \times \exp\left(-\frac{(R_c - \langle R_c\rangle)^2}{2\sigma_p^2 \langle R_c\rangle^2}\right), \tag{6}$$

$$\text{with } \langle V^2\rangle = \frac{1}{\sqrt{2\pi}\sigma_p \langle R_c\rangle} \int dR_c V^2(R_c) \exp\left(-\frac{(R_c - \langle R_c\rangle)^2}{2\sigma_p^2 \langle R_c\rangle^2}\right), \tag{7}$$

where $\langle R_c\rangle$ is the average radius of the core and $V(R) = 4\pi R^3/3$. Furthermore, we consider the particle inhomogeneity at length scales much smaller than the particle size due to the fact that the particle is made of cross-linked polymer chains. We take these inhomogeneities into account by including an additional term,

$$I_{\mathrm{chain}}(q) = \frac{I_{\mathrm{chain}}(0)}{1 + (\xi q)^2}, \tag{8}$$

with $I_{\mathrm{chain}}(0)$ the zero-q intensity of this contribution and ξ the correlation length or mesh size of the polymer network.[51] We emphasize that since the cross-linker concentration is spatially inhomogeneous within the particles, ξ is an estimate of the average mesh size. From the amount of cross-linker used in the particle synthesis, we estimate $\xi_H \approx (3.6 \pm 0.5)$ nm and $\xi_D \approx (5.4 \pm 0.7)$ nm using the relation

$$\xi = (N V_{p,d} / N_{\mathrm{x-link}})^{1/3}, \tag{9}$$

where N is the number of particles and $N_{\mathrm{x-link}}$ the number of cross-linker molecules. We estimate the number of particles from the calculated volume fraction of the total reaction yield in dilute conditions (using the conversion determined by viscometry) and the measured size of the particles. We note that it is difficult to determine ξ from fitting the SANS data, as $I_{\mathrm{chain}}(q)$ gives rise to a shallow decaying background that is noticeable at q-values beyond the steep decay of the scattering intensity.[50] As a result, we will fix a value of $\xi = 10$ nm for dilute measurements in our fits; this value represents the order of magnitude of the estimated and freely-fitted ξ. In concentrated samples, when $\zeta > 1$, we obtain the value of R_{SANS} and hence the particle volume $V_p = 4\pi R_{SANS}^3/3$ by fitting the form factor with ξ as a free parameter. However, we take as the representative value of ξ the one obtained from the dilute value, 10 nm, after considering a proportional decrease due to particle deswelling. Hence, for $\zeta > 1$, $\xi = (1/\zeta)^{1/3} \times 10$ nm.

With these considerations, we fit our data to the equation $I(q) \propto P(q) + I_{\mathrm{chain}}(q)$. From the fits, we obtain values of R_{SANS} that are in good agreement with the radii obtained from DLS, as shown in Table I. The polydispersities are found to be $\sigma_p = 0.14$ and $\sigma_p = 0.15$ for H-NIPAM and D-NIPAM suspensions. The measured fuzzy periphery, σ, of the D-NIPAM particles is smaller than that of the H-NIPAM particles, as also shown in Table I. This could result from different reaction kinetics associated with kinetic isotope effects: The different vibrational modes in the molecule depend on the mass of the nucleus of the constituent atoms. Since the electron cloud is coupled to the nuclei, the difference in vibrational motion results in associated differences in the electron cloud that can affect how polymerization proceeds. As a result, the reaction rate can depend on the type of nuclei in the molecule.[52,53] Moreover, these differences are enhanced due to the fact that ^{2}H hydrogen bonds are more stable than ^{1}H bonds.[54] Since the distribution of polymer and cross-linker in a microgel particle is determined by their reaction rate constants, these differences will change the detailed properties of the final microgel obtained.

SANS of concentrated suspensions

In highly concentrated samples, the pNIPAM particles must respond to the reduction of available volume per particle. Their softness and the high osmotic pressure in overpacked suspensions suggest that the particles deform and shrink once they can no longer fit into the available space, but it is not obvious whether interpenetration of the particles occurs. We study the response of the pNIPAM particles in highly packed conditions with eight tracer samples and six ZAC samples with different polymer concentrations as listed in Table I. To obtain the form factor from a SANS measurement, the proper background must be subtracted. For the tracer method, this background consists of D-NIPAM particles in H_2O / D_2O matching the scattering length density of those particles, while for the ZAC method the background

TABLE I. Sample details and structural parameters obtained from fits to SANS measurements using the model given by Eqs. (6) and (8) and shown in Figs. 5 and 6. The lengths R_{SANS}, R_c, σ, and ξ are given in nanometers. Tracer and ZAC samples are listed as $T\alpha$, with $\alpha = 1,\ldots,8$ and ZACα, with $\alpha = 1,\ldots,6$. All measurements were carried out at $T = 20\,^{\circ}$C.

Sample	c_p wt. %	ζ	R_{DLS} (dilute)	R_{SANS}	$\langle R_c \rangle$	2σ	σ_p	ξ
H1	0.39	0.08	149 ± 7	146 ± 3	104 ± 1.0	41.6 ± 2.0	0.14 ± 0.02	10.0
D1	0.24	0.12	136 ± 6	132 ± 3	109 ± 1.2	22.7 ± 1.9	0.15 ± 0.03	10.0
T1	1.25	0.55		149 ± 3	105 ± 1.0	44.4 ± 2.0	0.15 ± 0.01	9.93
T2	2.08	0.97		148 ± 3	104 ± 1.0	44.0 ± 2.0	0.15 ± 0.01	9.85
T3	2.44	1.15		145 ± 3	102 ± 1.0	43.2 ± 2.0	0.15 ± 0.01	9.67
T4	2.67	1.28		139 ± 5	103 ± 1.5	36.4 ± 3.0	0.16 ± 0.01	9.21
T5	2.93	1.41		132 ± 5	101 ± 1.5	31.0 ± 3.0	0.16 ± 0.01	8.78
T6	5.56	2.73		115 ± 6	89.7 ± 2	25.6 ± 4.0	0.19 ± 0.02	7.65
T7	6.06	3.01		112 ± 5	94.9 ± 1.5	17.0 ± 3.0	0.18 ± 0.01	7.32
T8	7.10	3.54		104 ± 3	90.7 ± 1.0	13.0 ± 2.0	0.17 ± 0.01	6.66
ZAC1	0.92	0.36		157 ± 6	117 ± 2.0	40.0 ± 4.0	0.21 ± 0.03	10.0
ZAC2	1.76	0.69		158 ± 5	116 ± 1.5	42.0 ± 3.0	0.21 ± 0.03	10.0
ZAC3	2.24	0.88		149 ± 3	111 ± 1.0	37.8 ± 2.0	0.20 ± 0.03	9.84
ZAC4	4.13	1.55		131 ± 3	98 ± 1.0	33.0 ± 2.0	0.20 ± 0.03	8.73
ZAC5	4.98	1.87		131 ± 3	100 ± 1.0	31.4 ± 2.0	0.20 ± 0.03	8.74
ZAC6	5.84	2.19		109 ± 3	82 ± 1.0	26.8 ± 2.0	0.20 ± 0.03	7.22

is given by the H_2O / D_2O mixture that contrast-matches a 50/50 mixture of H- and D-NIPAM particles. These backgrounds are measured in separate measurements to subtract them from the tracer and ZAC measurements.

The measured form factors are similar to those determined in dilute conditions, even if now the generalized volume fraction is close to and even larger than 1. The fits to the form factor model are equally good also, as shown in Fig. 6. The characteristic length scales of the particle, $\langle R_c \rangle$ (triangles) and 2σ (diamonds), and the overall size R_{SANS} (circles), obtained from the fits of the tracer experiment, all decrease for $\zeta \gtrsim 1$, as shown in Fig. 7. Deswelling thus begins when $\zeta \approx 1$. The decrease in R_{SANS} is mostly due to a reduction of the corona thickness, 2σ, which decreases by almost 65% as ζ increases from 1.0 to 3.6. The decrease in core radius is comparatively small; it is only reduced by about 13% for the same increase in ζ. The near-constant core size reflects the larger stiffness of the particle core due to the increased cross-linker concentration near the particle center.[55]

The ZAC measurements are consistent with this, as shown in Fig. 7. However, due to the difference in σ between H- and D-NIPAM particles, we do not expect the ZAC results to be as accurate as the tracer results, as both H- and D-NIPAM particles contribute to the form factor obtained with the ZAC method. Even if the smaller periphery of the D-NIPAM particles may indirectly influence $P_H(q)$ in the tracer experiment, there is no direct contribution to $P_H(q)$ from the D-NIPAM particles. By contrast, in the ZAC experiment, the particles directly and equally contribute to the measured form

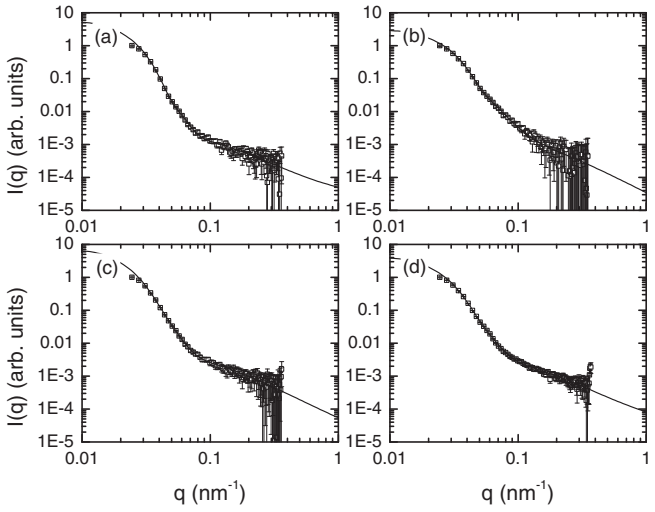

FIG. 6. Representative measured form factors of concentrated samples (open squares) and corresponding fits (lines) to Eqs. (6) and (8). The samples are (a) T2, (b) T7, (c) ZAC2, and (d) ZAC5 from Table I. As with the dilute samples, the fits are performed giving less statistical weight to the first point.

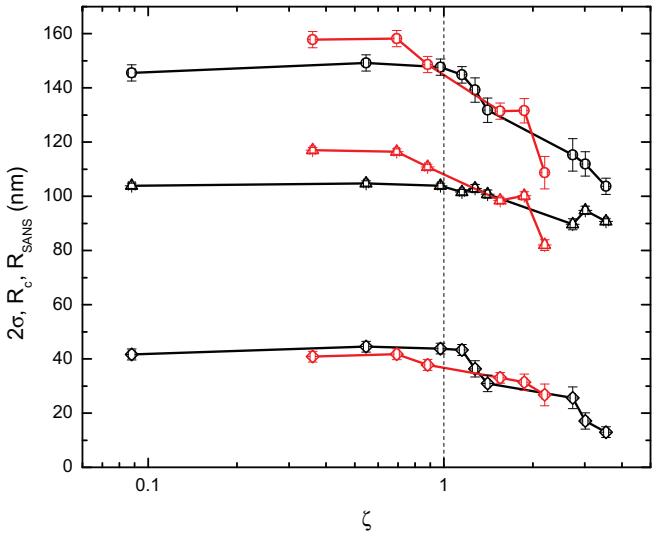

FIG. 7. Particle size from tracer (black) and ZAC (red) samples versus generalized volume fraction ζ. The total radius R_{SANS} (circles), the core radius $\langle R_c \rangle$ (triangles), and the fuzzy surface thickness 2σ (diamonds) are shown. Lines are guides to the eye.

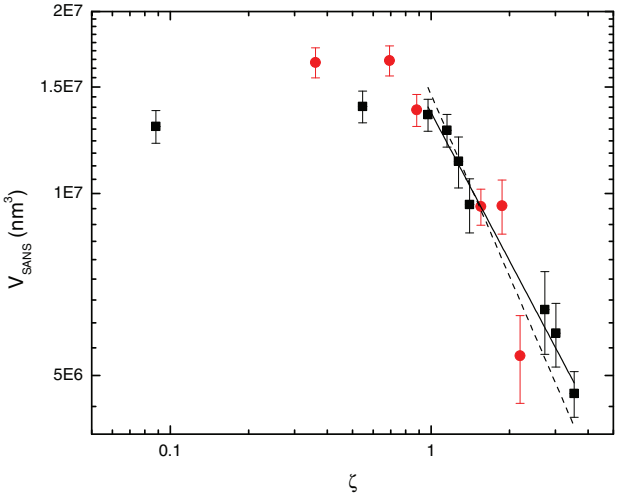

FIG. 8. Particle volume, V_{SANS}, as determined from tracer (black squares) and ZAC (red circles) samples as a function of effective volume fraction ζ. The lines show particle shrinkage according to $\propto\zeta^{-1}$ (dashed line) and $\propto\zeta^{-0.82\pm0.05}$ (solid line).

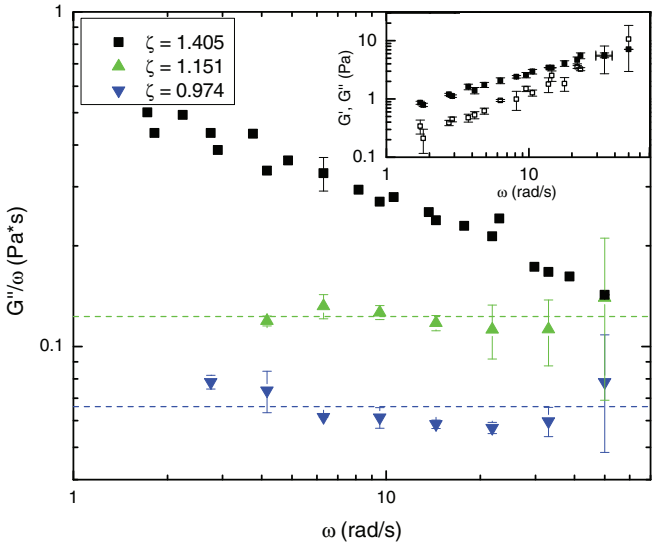

FIG. 9. G''/ω versus frequency for $\zeta = 0.974$ (blue downward triangles), $\zeta = 1.151$ (green upward triangles), and $\zeta = 1.405$ (black squares). The inset shows G' (open squares) and G'' (closed squares) for $\zeta = 1.405$; though all samples are liquid-like, the sample at $\zeta = 1.405$ has an appreciable contribution from G'. Lines are best fits to the data for frequency-independent viscosity.

factor, in addition to any indirect effects caused by the interactions between particles. Additionally, for the ZAC measurement, the solvent composition was determined from the experimentally determined matchpoints of both the H- and D-NIPAM particles, whereas for the tracer measurements, the solvent was determined only from the matchpoint of the D-NIPAM particles. This means that the SLD contrast between the H-particles and the solvent in the tracer experiments is between 3.3 and 4.7 Å^{-2}, while between the D-particles and the solvent the contrast is between 0 and 0.6 Å^{-2}. Following Eq. (4), the maximum possible contribution to the scattered intensity from the D-particles would be about 4% of the scattered intensity from the H-particles. However, taking the same uncertainties into account for the ZAC experiment gives a maximum difference in scattered intensity between the H- and D-particles of at least 300%. Thus, we are very confident about the accuracy of the contrast matching for the tracer measurements, but not so much for the ZAC measurements.

To quantify how the particle volume decreases with ζ, for $\zeta \geq 1$, we plot V_p versus ζ for tracer (black squares) and ZAC (red circles) samples in Fig. 8. The ZAC data are included for comparison only. A fit to the tracer data at $\zeta > 1$ without constraining the exponent gives $V \propto \zeta^{-0.82\pm0.05}$ (solid line) as best fit. However, constraining the volume to follow ζ^{-1} also describes the data reasonably well (dashed line). This may indicate that the particles are interpenetrating somewhat to fit into the available volume, in addition to deswelling, which is the dominant effect in our system. Furthermore, the particle volume is found to stay constant within the accuracy of the measurements for $\zeta \lesssim 1$. Apparently, the microgel particles maintain a constant size as the osmotic pressure of the suspension increases and are only forced to shrink when they are in close contact with their nearest neighbors, consistent with recent results.[17,27]

Rheology of concentrated suspensions

Our SANS results clearly show there is no concentration-induced deswelling for our particles until $\zeta \sim 1$. We also do not observe crystal formation within the ζ-range explored; this could result from suspension polydispersity,[56] although particle softness[57] and possible differences in structure of the fuzzy periphery of H- and D-particles could also play a role. To explore whether the system is a liquid or a glass, we first perform oscillatory rheology in the linear regime, where both the elastic and viscous moduli, G' and G'', respectively, are independent of the applied strain. For $\zeta = 0.79$ and $\zeta = 1.15$, $G'' \gg G'$ indicating the liquid-like character of these samples. Indeed, for a liquid, the viscous modulus $G'' = \eta\omega$, and so G''/ω is a constant irrespective of frequency, as shown in Fig. 9. However, at $\zeta = 1.41$, the viscous modulus is no longer linear in ω, as also shown in Fig. 9, and the elastic modulus G' is now measurable and close in value to G'', as shown in the inset of Fig. 9. Hence, the sample exhibits viscoelastic behavior in the probed frequency range at this ζ.

We also perform steady-state rheology and determine the suspension viscosity, η, as a function of shear rate, $\dot{\gamma}$, for different ζ. We observe an increasing shear thinning behavior as ζ increases, as shown in Fig. 10. The data are well described by the Cross model,[58]

$$\eta - \eta_\infty = \frac{\eta_0 - \eta_\infty}{1 + (\frac{\dot{\gamma}}{\dot{\gamma}_c})^n}, \tag{10}$$

where η_0 and η_∞ are the zero-shear-rate and infinite-shear-rate viscosities, respectively, $\dot{\gamma}_c$ is a critical shear rate corresponding to a viscosity that is halfway between η_0 and η_∞, and n is a parameter controlling the sharpness of the transition. From the fits to the data, we obtain the values of these parameters, except η_∞. Since we do not have enough data

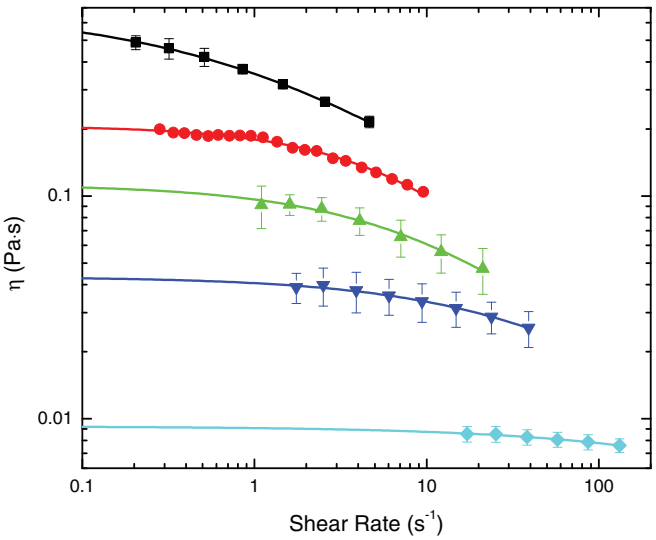

FIG. 10. Viscosity plotted as a function of shear rate for different values of ζ. Solid lines are the fits to the data using the Cross model. The volume fractions are $\zeta = 1.405$ (black squares), $\zeta = 1.275$ (red circles), $\zeta = 1.151$ (green upward triangles), $\zeta = 0.974$ (blue downward triangles), and $\zeta = 0.547$ (cyan diamonds).

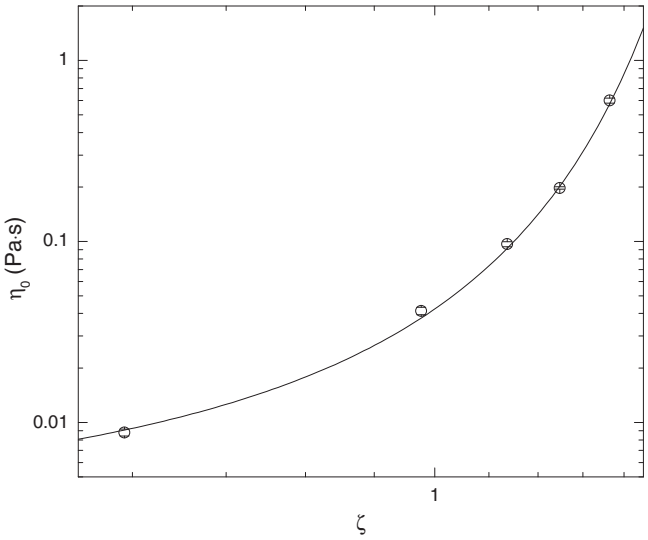

FIG. 11. Zero-shear-rate viscosity versus ζ. The line is a fit to the Vogel-Fulcher-Tammann function.

points at high shear rates, the fits are insensitive to the value of η_∞, which as a result cannot be determined without significant error. This is clearly reflected in the fact that the error in $\dot{\gamma}_c$ increases with decreasing ζ.

We find that the values of η_0 compare well with the oscillatory results, as shown in Table II. The exponent n is around 1, with no clear ζ dependence. From $\dot{\gamma}_c$, we estimate the advective timescale, $1/\dot{\gamma}_c$, and obtain a critical Péclet number:

$$Pe_c = \frac{6\pi\eta_s R_{SANS}^3}{k_B T}\dot{\gamma}_c \tag{11}$$

that compares the ratio between the diffusive timescale, R_{SANS}^2/D, and the advective timescale, with D the diffusion coefficient calculated according to the Stokes-Einstein equation.

In general, colloidal suspensions shear-thin when $Pe_c \gtrsim 1$. However, as the particles begin interfering with one another hydrodynamically, the diffusion coefficient is not well-described by the Stokes-Einstein equation and shear thinning occurs at lower and lower Péclet numbers as the volume fraction increases.[59] This is exactly what we observe: The value of Pe_c indeed decreases with increasing ζ, indicating an increasing interaction between the particles.

Interestingly, the ζ-dependence of the zero-shear-rate viscosity is well described by a Vogel-Fulcher-Tammann function,[60] $\eta_0 = A\exp[B\zeta/(\zeta_0 - \zeta)]$, where ζ_0 sets the apparent divergence of η_0, B controls the growth of η_0 on approach to ζ_0, and A is the suspension viscosity for low values of ζ (see Fig. 11). This empirical function describes the ζ dependence of the viscosity of microgel suspensions near their glass transition[11] and, with $1/\zeta$ exchanged for temperature, it also provides a good description of the T dependence of the viscosity for supercooled molecular liquids on their approach to the glass.[60] From the fit, we find $A = (3.1 \pm 0.6)10^{-3}$ Pa s, which is of the same order as the viscosity of water, $B = 3.6 \pm 0.7$, and $\zeta_0 = 2.4 \pm 0.2$. We emphasize that similar results are obtained, if models other than the Cross model are used to describe the viscosity dependence with shear rate to extract the zero-shear-rate viscosity; we have confirmed this using the model by Carreau,[61] Powell-Eyring (see Ref. 62), and Johnson (see Ref. 63).

Note that in contrast to some other systems with soft particle interactions,[64] our microgel suspensions remain liquid-like well above $\zeta \approx 1$, corresponding to where the microgel particles begin to appreciably deswell. This high mobility at high ζ emphasizes the importance of single-particle softness

TABLE II. Values of η_0, $\dot{\gamma}_c$, and n for several tracer samples determined by fitting the flow curves in Fig. 10 using Eq. (10). For comparison, we also list the viscosities determined from oscillatory measurements for samples displaying purely liquid-like behavior; these values represent another way of measuring the zero-shear-rate viscosity. Also listed are Péclet numbers calculated according to Eq. (11) at the critical shear rate using R_H as the particle radius. Viscosities are given in units of 10^{-3} Pa s and $\dot{\gamma}_c$ in units of s^{-1}.

Sample	ζ	η_0 (Cross)	η_0 (Oscillatory)	$\dot{\gamma}_c$	Pe_c	n
T5	1.41	600 ± 19		1.13 ± 0.05	$(1.44 \pm 0.24) \times 10^{-2}$	0.76 ± 0.06
T4	1.28	197 ± 3		3.7 ± 0.6	$(5.6 \pm 1.5) \times 10^{-2}$	1.38 ± 0.20
T3	1.15	97 ± 3	123 ± 24	6.3 ± 0.7	$(1.07 \pm 0.21) \times 10^{-1}$	1.6 ± 0.3
T2	0.97	41.3 ± 2.0	66 ± 12	21 ± 13	$(4 \pm 3) \times 10^{-1}$	1.0 ± 0.4
T1	0.55	8.8 ± 0.4	15 ± 8	86 ± 80	1.7 ± 1.6	1.3 ± 1.2

and supports the conclusion that the slower viscosity increase with concentration, as compared to that of hard sphere suspensions, could be traced back to the intrinsic softness of the individual microgel particles.

CONCLUSIONS

The presented form factor data show that our pNIPAM microgel particles cross-linked with 2 mol. % BIS keep their fully swollen size up to generalized volume fractions $\zeta \approx 1$ in spite of the increasing osmotic pressure of the suspension: only at $\zeta \gtrsim 1$ are they forced to shrink, with some interpenetration. Our rheology further confirms that particle softness is responsible for the persistent liquid-like behavior of our suspensions above $\zeta = 1$, where the suspension is in overpacked condition. To the best of our knowledge, the presented form factor data give the first direct determination of the form factor of microgel particles under highly packed conditions. Our results allow for an improved interpretation of scattering data obtained at $\zeta \gtrsim 1$, which has been hampered by the unknown change of the form factor in these conditions.

ACKNOWLEDGMENTS

Financial support from the ACS Petroleum Research Fund (PRF 50603-DNI7) and the Swiss National Science Foundation (Grant No. 200021-132128) is gratefully acknowledged. SANS measurements were carried out on the instruments SANS-I and SANS-II at SINQ, Paul Scherrer Institut, Switzerland.

[1]R. Pelton, Adv. Colloid Interface Sci. **85**, 1 (2000).
[2]J. J. Lietor-Santos, B. Sierra-Martin, R. Vavrin, Z. Hu, U. Gasser, and A. Fernandez-Nieves, Macromolecules **42**, 6225 (2009).
[3]A. Fernandez-Nieves, A. Fernandez-Barbero, B. Vincent, and F. J. de las Nieves, Macromolecules **33**, 2114 (2000).
[4]A. Fernandez-Nieves, A. Fernandez-Barbero, and F. J. de las Nieves, J. Chem. Phys. **115**, 7644 (2001).
[5]A. Fernandez-Nieves, A. Fernandez-Barbero, B. Vincent, and F. J. de las Nieves, J. Chem. Phys. **119**, 10383 (2003).
[6]D. J. Beebe, J. S. Moore, J. M. Bauer, Q. Yu, R. H. Liu, C. Devadoss, and B.-H. Jo, Nature (London) **404**, 588 (2000).
[7]S. V. Vinogradov, T. K. Bronich, and A. V. Kabanov, Adv. Drug Delivery Rev. **54**, 135 (2002).
[8]M. J. Serpe, J. Kim, and L. A. Lyon, Adv. Mater. **16**, 184 (2004).
[9]B. R. Saunders and B. Vincent, Adv. Colloid Interface Sci. **80**, 1 (1999).
[10]A. M. Alsayed, M. F. Islam, J. Zhang, P. J. Collings, and A. G. Yodh, Science **309**, 1207 (2005).
[11]J. Mattsson, H. M. Wyss, A. Fernandez-Nieves, K. Miyazaki, Z. Hu, D. R. Reichman, and D. A. Weitz, Nature (London) **462**, 83 (2009).
[12]D. Stamenovic, J. Colloid Interface Sci. **145**, 255 (1991).
[13]T. G. Mason, J. Bibette, and D. A. Weitz, Phys. Rev. Lett. **75**, 2051 (1995).
[14]K. de Haas, C. Blom, D. van den Ende, M. Duits, B. Haveman, and J. Mellema, Langmuir **13**, 6658 (1997).
[15]T. G. Mason and D. A. Weitz, Phys. Rev. Lett. **75**, 2770 (1995).
[16]J. R. Seth, L. Mohan, C. Locatelli-Champagne, M. Cloitre, and R. T. Bonnecaze, Nat. Mater. **10**, 838 (2011).
[17]J. Lietor-Santos, B. Sierra-Martin, and A. Fernandez-Nieves, Phys. Rev. E **84**, 060402(R) (2011).
[18]M. Destribats, V. Lapeyre, M. Wolfs, E. Sellier, F. Leal-Calderon, V. Ravaine, and V. Schmitt, Soft Matter **7**, 7689 (2011).
[19]K. Liu, D. Williams, and B. Briscoe, J. Phys. D: Appl. Phys. **31**, 294 (1998).
[20]M. Wolfe and C. Scopazzi, J. Colloid Interface Sci. **133**, 265 (1989).
[21]J. R. Stokes, "Rheology of industrially relevant microgels," in *Microgel Suspensions*, edited by A. Fernandez-Nieves, H. Wyss, J. Mattsson, and D. A. Weitz (WILEY-VCH Verlag GmbH and Co. KGaA, Weinheim, Germany, 2011), pp. 327–353.
[22]L. Berthier and T. Witten, EPL **86**, 10001 (2009).
[23]B. H. Tan, K. C. Tam, Y. C. Lam, and C. B. Tan, Polymer **45**, 5515 (2004).
[24]M. Cloitre, R. Borrega, F. Monti, and L. Leibler, C. R. Phys. **4**, 221 (2003).
[25]R. Borrega, M. Cloitre, I. Betremieux, B. Ernst, and L. Leibler, Europhys. Lett. **47**, 729 (1999).
[26]B. Tan, K. Tam, Y. Lam, and C. Tan, J. Rheol. **48**, 915 (2004).
[27]G. Romeo, L. Imperiali, J.-W. Kim, A. Fernandez-Nieves, and D. A. Weitz, J. Chem. Phys. **136**, 124905 (2012).
[28]M. Stieger, J. Pedersen, P. Lindner, and W. Richtering, Langmuir **20**, 7283 (2004).
[29]Z. Ahmed, E. A. Gooding, K. V. Pimenov, L. L. Wang, and S. A. Asher, J. Phys. Chem. B **113**, 4248 (2009).
[30]J. K. G. Dhont, *An Introduction to Dynamics of Colloids* (Elsevier, 1996).
[31]A. Einstein, Ann. Phys. (Berlin, Ger.) **322**, 549 (1905).
[32]M. Shibayama, T. Tanaka, and C. C. Han, J. Chem. Phys. **97**, 6829 (1992).
[33]A. Fernandez-Barbero, A. Fernandez-Nieves, I. Grillo, and E. Lopez-Cabarcos, Phys. Rev. E **66**, 051803 (2002).
[34]B. R. Saunders, Langmuir **20**, 3925 (2004).
[35]A. Routh and W. Zimmerman, J. Colloid Interface Sci. **261**, 547 (2003).
[36]E. H. Purnomo, D. van den Ende, S. A. Vanapalli, and F. Mugele, Phys. Rev. Lett. **101**, 238301 (2008).
[37]D. van den Ende, E. Purnomo, M. Duits, W. Richtering, and F. Mugele, Phys. Rev. E **81**, 011404 (2010).
[38]E. H. Purnomo, D. van den Ende, J. Mellema, and F. Mugele, Phys. Rev. E **76**, 021404 (2007).
[39]V. Breedveld, D. van den Ende, and R. Jongschaap, J. Chem. Phys. **114**, 5923 (2001).
[40]L. Willner, O. Jucknischke, D. Richter, J. Roovers, L.-L. Zhou, P. Toporowski, L. Fetters, J. Huang, M. Lin, and N. Hadjichristidis, Macromolecules **27**, 3821 (1994).
[41]G. D. Wignall and Y. B. Melnichenko, Rep. Prog. Phys. **68**, 1761 (2005).
[42]A. Munter, NIST Center for Neutron Research, see http://www.ncnr.nist.gov/resources/activation (June 2014).
[43]V. Sears, Neutron News **3**, 26 (1992).
[44]M. Reufer, P. Diaz-Leyva, I. Lynch, and F. Scheffold, Eur. Phys. J. E **28**, 165 (2009).
[45]R. P. May, *Neutron Data Booklet* (Old City Publishing, Philadelphia, USA, 2003), p. 2.1.
[46]J. S. Higgins and H. C. Benoît, *Polymers and Neutron Scattering* (Oxford University Press Inc., New York, 1994).
[47]P. Lindner, in *Neutrons, X-Rays and Light: Scattering Methods Applied to Soft Condensed Matter*, edited by P. Lindner, and T. Zemb (Elsevier, Amsterdam, 2002).
[48]M. Stieger, W. Richtering, J. Pedersen, and P. Lindner, J. Chem. Phys. **120**, 6197 (2004).
[49]T. Hellweg, C. D. Dewhurst, E. Brueckner, K. Kratz, and W. Eimer, Colloid Polym. Sci. **278**, 972 (2000).
[50]J. J. Lietor-Santos, U. Gasser, R. Vavrin, Z. Hu, and A. Fernandez-Nieves, J. Chem. Phys. **133**, 034901 (2010).
[51]V. Prabhu, M. Muthukumar, G. Wignall, and Y. Melnichenko, Polymer **42**, 8935 (2001).
[52]E. V. Anslyn and D. A. Dougherty, *Modern Physical Organic Chemistry* (University Science Books, Sausalito, California, 2006).
[53]C. Hennig, R. Oswald, and S. Schmatz, J. Phys. Chem. A **110**, 3071 (2006).
[54]H. Shirota, N. Kuwabara, K. Ohkawa, and K. Horie, J. Phys. Chem. B **103**, 10400 (1999).
[55]X. Wu, R. Pelton, A. Hamielec, D. Woods, and W. McPhee, Colloid Polym. Sci. **272**, 467 (1994).
[56]P. Chaudhuri, S. Karmakar, C. Dasgupta, H. R. Krishnamurthy, and A. K. Sood, Phys. Rev. Lett. **95**, 248301 (2005).
[57]B. Sierra-Martin and A. Fernandez-Nieves, Soft Matter **8**, 4141 (2012).
[58]M. Cross, J. Colloid Sci. **20**, 417 (1965).
[59]J. van der Werff, C. de Kruif, and J. Dhont, Physica A **160**, 205 (1989).
[60]C. A. Angell, K. L. Ngai, G. B. McKenna, P. F. McMillan, and S. W. Martin, J. Appl. Phys. **88**, 3113 (2000).
[61]P. Carreau, Trans. Soc. Rheol. **16**, 99 (1972).
[62]E. Christiansen, N. Ryan, and W. Stevens, AIChE J. **1**, 544 (1955).
[63]P. Xu, T. Cagin, and W. Goddard III, J. Chem. Phys. **123**, 104506 (2005).
[64]P. Nommensen, M. Duits, D. van den Ende, and J. Mellema, Phys. Rev. E **59**, 3147 (1999).